



International Conference On Medical Imaging Understanding and Analysis 2016, MIUA 2016,
6-8 July 2016, Loughborough, UK

Fast Automated Liver Delineation from Computational Tomography Angiography

Xiaowei Ding^{a,c,*}, Xin Geng^b, Chenfanfu Jiang^c, Feng Tian^d, Xingjian Yan^c, Hang Qi^c,
Lei Zhang^e, Yongchang Zheng^f

^a*VoxelCloud Inc., 505 N Figueroa St. Suite 514, Los Angeles 90012, USA*

^b*Department of Cardiothoracic Surgery, Huashan Hospital of Fudan University, 12 Middle Urumqi Road, Shanghai 200040, China*

^c*Computer Science Department, Henry Samueli School of Engineering and Applied Science at UCLA, 580 Portola Plaza, Los Angeles 90095, USA*

^d*Clinical Medicine Department, Shanghai Jiao Tong University School of Medicine, 280 Chongqing S Rd, Shanghai 200025, China*

^e*Department of Radiology, Shanghai East Hospital, 150 Jimo Rd. Shanghai 200120, China*

^f*Department of Liver Surgery, Chinese Academy of Medical Sciences and Peking Union Medical College, 1 Shuaifuyuan, Beijing 100730, China*

Abstract

Accurate liver segmentation is essential for surgery planning and diagnosis of liver abnormality with algorithms. We propose and validate a multi-atlas segmentation approach with local decision fusion for fast automated liver (with/without abnormality) segmentation on computational tomography angiography (CTA). Thirty-five patients were enrolled in this study. A co-registered segmented CTA atlas is constructed with 20 CTA scans, normal and abnormal subjects with wide range of body-mass index (BMI). Liver segmentation candidates are achieved by a multi-atlas registration algorithm which propagates the segmentation label on each atlas image to the test image by image registration. The final segmentation result is calculated by applying local decision fusion weights to each propagated candidate segmentation. We applied our algorithm on the rest 15 patients and compared them with manual segmentation by two expert readers. Voxel overlap by Dice coefficient between the algorithm and expert readers was 0.93 (range 0.89 - 0.94). The mean surface distance and Hausdorff distance in millimeters between manually drawn contours and the automatically obtained contours were 1.1 ± 0.9 mm and 5.9 ± 1.7 mm respectively. Using our approach, physicians can accurately segment liver from CTA without tedious manual tracing. Our automated algorithm for liver segmentation achieved accurate segmentation with/without abnormality.

© 2016 The Authors. Published by Elsevier B.V. This is an open access article under the CC BY-NC-ND license (<http://creativecommons.org/licenses/by-nc-nd/4.0/>).

Peer-review under responsibility of the Organizing Committee of MIUA 2016

Keywords: Liver; segmentation; computational tomography angiography; atlas; registration;

1. Introduction

Liver segmentation is essential for surgery planning and computer-aided diagnosis. Liver segmentation from CT images is more challenging compared to other abdominal organ segmentation. First, intensity distributions between

* Corresponding author. Tel.: +1-310-499-3064 ;
E-mail address: xiaowei@cs.ucla.edu

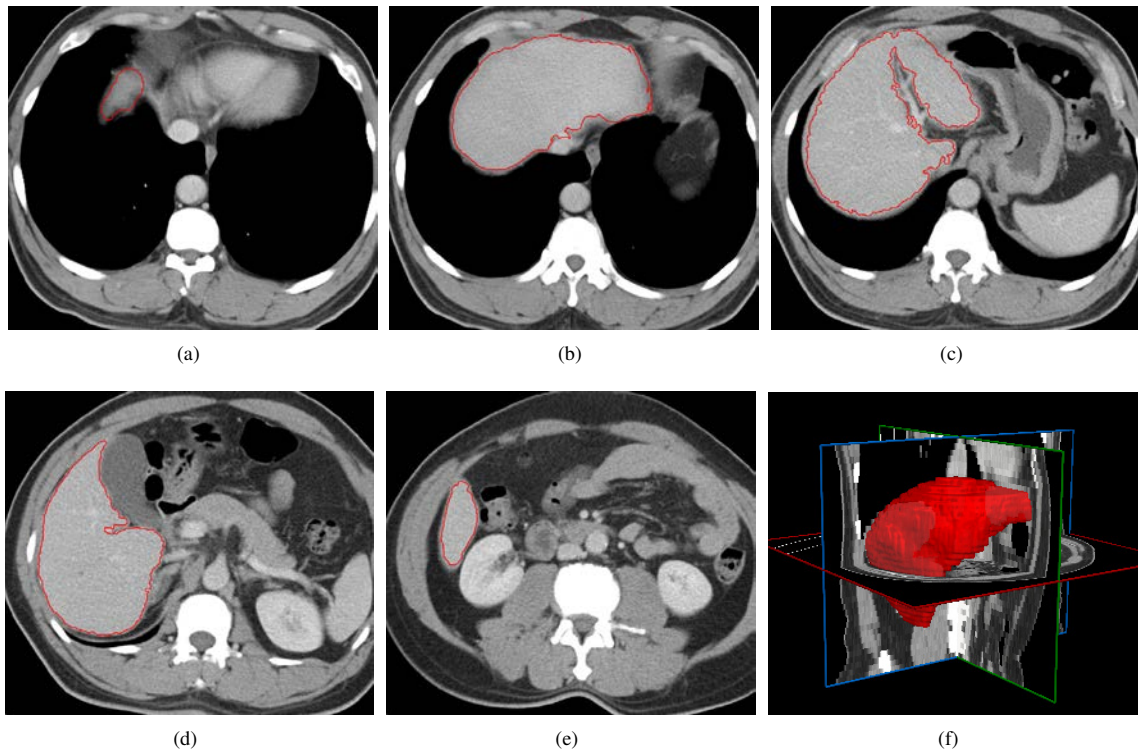


Fig. 1. Example of atlas images and manual tracing of liver region. (a)-(e) 2D contours on transverse slices within upper and lower limits of liver, (f) 3D mask created from the 2D contours.

the liver and its nearby organs are similar. Moreover, different livers, especially abnormal ones, have varied shapes. Thus, fully-automated liver segmentation is still an open problem.

Several investigators have reported methods for liver segmentation on CT data. Gao¹ extracted information from the global histogram of abdominal CT images and combined morphological operators to define the liver area. This intensity-based method is unstable in the area of the liver boundary where fuzzy voxel intensity is present. Luo² extracted pixel-level features of wavelet coefficients and Haralick texture descriptors³, classified the data into pixel-wise liver or non-liver by support vector machines and combined morphological operations to delineate the liver. Militzer⁴ designed strong and compact classifiers for feature classification based on the AdaBoost algorithm and Probabilistic Boosting Trees to get high accuracy for liver tumors segmentation. These methods are relatively simple in the process of target region refinement, and only based on morphological filtering. Statistical shape models are also applied to liver segmentation to overcome the over-segmentation problem of intensity and texture based methods. Zhang⁵ used a statistical shape model driven by optimal surface detection. Okada⁶ fused a probabilistic atlas and multilevel statistical shape model to integrate global shape and appearance features of abdominal CT images for liver segmentation.

In this paper, we present an automated liver segmentation method that can handle livers with/without abnormality based on a fast multi-atlas based method. The experimental results demonstrate that compared to expert manual tracing, the proposed method is significantly effective and robust for the segmentation of liver from CTA images.

2. Method

In this section, we first describe the image acquisition protocol, followed by the creation of the liver CTA atlases. Next, we present the proposed liver segmentation algorithm.

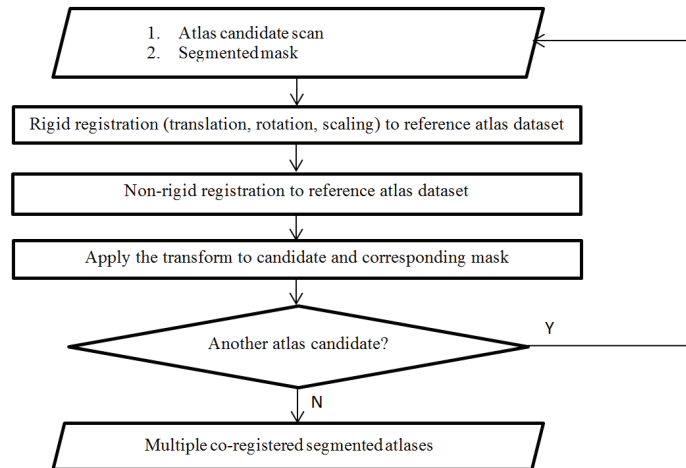


Fig. 2. Flowchart of the atlas creation procedure.

2.1. Image data

We analyzed CTA data collected for liver screening, at the Peking Union Medical College Hospital, China. Each CT dataset comprised 50 to 60 image slices with a resolution of 512×512 pixels of size $0.68 \times 0.68 \text{ mm}^2$ and a slice thickness of 5.0 mm. The datasets were selected from consecutive, both symptomatic and asymptomatic patients undergoing liver screening, and they were free of motion artifacts.

2.2. Algorithm

2.2.1. Overview

A CTA atlas was first created from multiple co-registered CTA datasets ($N=20$; 10 men and 10 women) in which the liver region were manually segmented (Figure 2 a-e) in the following way: on all transverse slices, 2D contours were manually traced by expert readers within the superior and inferior limits of the liver; a 3D binary volume mask was generated from the 2D contours (Figure 2 f). After the atlas was created, the algorithm registers the primary atlas to the test CTA data to get the non-rigid transformation for segmentation label propagation. The implementation of the multiple registrations is largely based on the earlier work on multi-atlas-based methods^{7,8}. To get the final segmentation result, labels on all the atlases were propagated to the test data by applying the same non-rigid transformation, and the fusion of those propagated labels on the test CTA data are calculated according to spatially varying decision fusion weights^{7,9,10,11,12}.

2.2.2. Multiple atlas registration

The rigid and nonrigid registration problem is formulated as an optimization problem with respect to combined affine and B-spline transformations μ minimizing the difference between the target images and the reference image:

$$\hat{\mu} = \arg \min_{\mu} C[\mu; U(\mathbf{p}), A(\mathbf{p})], \quad (1)$$

where $\hat{\mu}$ is the transformation aligning atlas $A(\mu(\mathbf{p}))$ to target image $U(\mathbf{p})$, \mathbf{p} denotes a voxel, and C is the negative mutual information¹³. Image registration is used in both atlas creation and target image segmentation.⁷ used a one-to-all registration scheme between the target image and the atlas; however, the time required to register the target image to every image in the atlas is prohibitive for clinical practice. To speed up the registration process, we co-register the atlas images to a single primary image when the atlases are created, and then the computed transform between target image and the atlas primary image is applied to all the images in the atlas in order to segment the target image. This will cost only $1/N$ of the time that one-to-all registration needs, where N is the number of subjects in the atlas. The

atlases incorporate prior information and may be modified by users who need something closer to their own data. This registration step determines the location and shape of the liver. To obtain the rough binary segmentation of the liver $S(\mathbf{p})$, the labels S_i are propagated to the test image using weights that are related to the contribution of each atlas by measuring the similarity of their registration results after transformation μ^7 . The relative importance of each atlas image is measured by the absolute difference D_i between the transformed moving atlas and the target image:

$$D_i(\mathbf{p}) = |A_i(\mu(\mathbf{p})) - U(\mathbf{p})|, \forall i. \quad (2)$$

To determine how much a propagated label in each atlas image should contribute to the segmentation, weights λ_i were calculated as follows:

$$\lambda_i(\mathbf{p}) = \frac{1}{D_i(\mathbf{p}) \times g_{\sigma_1}(\mathbf{p}) + \epsilon}, \quad (3)$$

where $g_{\sigma_1}(\mathbf{p})$ is a Gaussian kernel of scale sigma that smooths the local estimate of the registration, and ϵ is a small value to avoid division by zero. The resulting propagation label is determined by a weighted average of the transformed binary segmentation $S_i(\mu)$:

$$S(\mathbf{p}) = \frac{1}{\sum_{i=1}^N \lambda_i(\mathbf{p})} \sum_{i=1}^N \lambda_i(\mathbf{p}) S_i(\mu_i(\mathbf{p})) \quad (4)$$

To obtain a closed contour (Figure 4a-c), $S(\mathbf{p})$ was first blurred with a Gaussian kernel followed by thresholding at value 0.5.

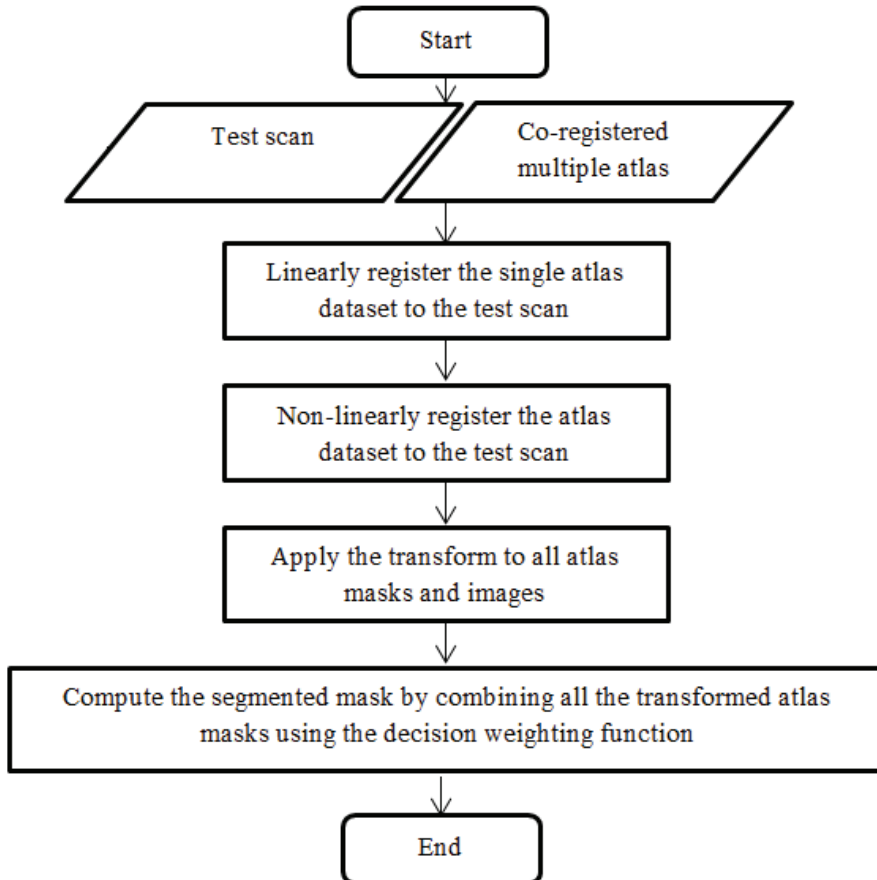


Fig. 3. Flowchart of the segmentation algorithm

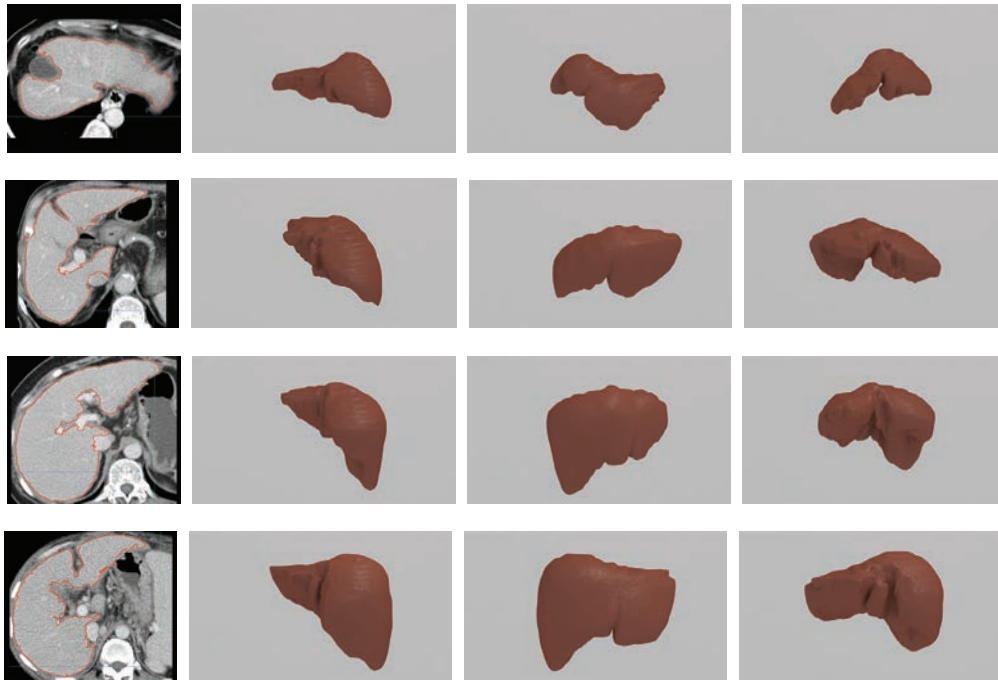


Fig. 4. Example of segmentation results on 2D transverse image slices and rendering of the reconstructed 3D liver mask of four patients. Each row represents one patient.

3. Results

To compare the automatic segmentation results with expert manual ones, two experienced radiologists, using consensus reading, manually traced the liver region for all 35 test CT datasets. Twenty were used to create the CTA atlas and the rest 15 for testing. Dice coefficient, surface distance and Hausdorff distance were used to compare the liver region obtained by our algorithm to the ground truth determined by expert manual tracing.

The mean Dice coefficient was 0.93 (range 0.89 - 0.94). The mean surface distance and Hausdorff distance in millimeter between manually drawn contours and the automatically obtained contours were 1.1 ± 0.9 mm and 5.9 ± 1.7 mm respectively. Four examples of segmentation results are shown in Figure 4, with rendering of the 3D liver mask. These cases with different extend of abnormality are well handled by our algorithm. The segmentation takes approximately 25 seconds of compute time on a standard workstation.

4. Conclusion

We have demonstrated that a fast algorithm for liver segmentation from contrast-enhanced CT is feasible and that it achieves 0.9316 Dice overlap with expert manual tracing in approximately 25 seconds of compute time on a standard workstation. Our fast atlas registration and proves to be effective for the accurate segmentation of weak image features such as similar intensity distribution between liver and its nearby organs, while it preserves the location and shape of the anatomical structure of interest.

References

1. Gao, L., Heath, D.G., Kuszyk, B.S., Fishman, E.K.. Automatic liver segmentation technique for three-dimensional visualization of ct data. *Radiology* 1996;**201**(2):359–364.
2. Luo, S., Jin, J.S., Chalup, S.K., Qian, G.. A liver segmentation algorithm based on wavelets and machine learning. In: *Computational Intelligence and Natural Computing, 2009. CINC'09. International Conference on*; vol. 2. IEEE; 2009, p. 122–125.

3. Semler, L., Dettori, L., Furst, J.. Wavelet-based texture classification of tissues in computed tomography. In: *Computer-Based Medical Systems, 2005. Proceedings. 18th IEEE Symposium on*. IEEE; 2005, p. 265–270.
4. Militzer, A., Hager, T., Jäger, F., Tietjen, C., Hornegger, J.. Automatic detection and segmentation of focal liver lesions in contrast enhanced ct images. In: *Pattern Recognition (ICPR), 2010 20th International Conference on*. IEEE; 2010, p. 2524–2527.
5. Zhang, X., Tian, J., Deng, K., Wu, Y., Li, X.. Automatic liver segmentation using a statistical shape model with optimal surface detection. *Biomedical Engineering, IEEE Transactions on* 2010;**57**(10):2622–2626.
6. Okada, T., Shimada, R., Hori, M., Nakamoto, M., Chen, Y.W., Nakamura, H., et al. Automated segmentation of the liver from 3d ct images using probabilistic atlas and multilevel statistical shape model. *Academic radiology* 2008;**15**(11):1390–1403.
7. Isgum, I., Staring, M., Rutten, A., Prokop, M., Viergever, M.A., van Ginneken, B.. Multi-atlas-based segmentation with local decision fusion: Application to cardiac and aortic segmentation in CT scans. *Medical Imaging, IEEE Transactions on* 2009;**28**(7):1000–1010.
8. Rueckert, D., Sonoda, L.L., Hayes, C., Hill, D.L., Leach, M.O., Hawkes, D.J.. Nonrigid registration using free-form deformations: Application to breast MR images. *Medical Imaging, IEEE Transactions on* 1999;**18**(8):712–721.
9. Ding, X., Slomka, P.J., Diaz-Zamudio, M., Germano, G., Berman, D.S., Terzopoulos, D., et al. Automated coronary artery calcium scoring from non-contrast CT using a patient-specific algorithm. In: *SPIE Medical Imaging*. International Society for Optics and Photonics; 2015, p. 94132U–94132U.
10. Ding, X., Terzopoulos, D., Diaz-Zamudio, M., Berman, D.S., Slomka, P.J., Dey, D.. Automated epicardial fat volume quantification from non-contrast CT. In: *SPIE Medical Imaging*. International Society for Optics and Photonics; 2014, p. 90340I–90340I.
11. Ding, X., Pang, J., Ren, Z., Diaz-Zamudio, M., Berman, D.S., Li, D., et al. Automated pericardial fat quantification from coronary magnetic resonance angiography. In: *Medical Image Understanding and Analysis*. MIUA; 2015, p. 80–85.
12. Ding, X., Terzopoulos, D., Diaz-Zamudio, M., Berman, D.S., Slomka, P.J., Dey, D.. Automated pericardium delineation and epicardial fat volume quantification from noncontrast CT. *Medical Physics* 2015;**42**(9):5015–5026.
13. Thévenaz, P., Unser, M.. Optimization of mutual information for multiresolution image registration. *Image Processing, IEEE Transactions on* 2000;**9**(12):2083–2099.